

Absorption and scattering by bispheres, quadspheres, and circular rings of spheres and their equivalent coated spheres

Ri-Liang Heng, Ki Cheong Sy, and Laurent Pilon*

Mechanical and Aerospace Engineering Department, Henry Samueli School of Engineering and Applied Science, University of California, Los Angeles 420 Westwood Plaza, Eng. IV 37-132, Los Angeles, California 90095, USA

*Corresponding author: pilon@seas.ucla.edu

Received July 25, 2014; accepted October 22, 2014;
posted November 7, 2014 (Doc. ID 217647); published December 4, 2014

This study demonstrates that the absorption and scattering cross sections and asymmetry factor of randomly oriented and optically soft bispheres, quadspheres, and circular rings of spheres, with either monodisperse or polydisperse monomers, can be approximated by an equivalent coated sphere with identical volume and average projected area. This approximation could also apply to the angle-dependent scattering matrix elements for monomer size parameter less than 0.1. However, it quickly deteriorated with increasing monomer number and/or size parameter. It was shown to be superior to previously proposed approximations considering a volume equivalent homogeneous sphere and a coated sphere with identical volume and surface area. These results provide a rapid and accurate way of predicting the radiation characteristics of bispheres, quadspheres, and rings of spheres representative of various unicellular and multicellular cyanobacteria considered for producing food supplements, biofuels, and fertilizers. They could also be used in inverse methods for retrieving the monomers' optical properties, morphology, and/or concentration. © 2014 Optical Society of America

OCIS codes: (010.5620) Radiative transfer; (010.4450) Oceanic optics; (290.5825) Scattering theory; (290.5855) Scattering, polarization; (290.7050) Turbid media; (100.3200) Inverse scattering.
<http://dx.doi.org/10.1364/JOSAA.32.000046>

1. INTRODUCTION

There are thousands of photosynthetic micro-organism species classified as diatoms, green or red microalgae, eustigmatophytes, prymnesiophytes, and cyanobacteria [1,2]. Certain species are capable of producing nutritional supplements [3], biofuels such as hydrogen [4] or lipids for biodiesel production [5], as well as fertilizers [3,6]. Other species are able to remove organic waste from effluent water [3]. While most diatoms and green microalgae exist in unicellular forms, cyanobacteria can be either unicellular or multicellular [7,8]. For example, *Synechocystis sp.* is a unicellular cyanobacterium with a dumbbell shape. It was the first photosynthetic organism whose entire genome was sequenced [9]. It has been used as a model organism to study photosynthesis, pigment synthesis, carbon and nitrogen assimilation, lipid production, and other metabolic processes [9–12]. Figure 1(a) shows a micrograph of a population of free-floating *Synechocystis sp.* cells about 3 to 5 μm in length. Figure 1(b) shows a micrograph of *Synechocystis sp.* immediately after cell division into two morphologically identical daughter cells [13]. On the other hand, certain multicellular cyanobacteria, such as *Anabaena elenkinii* and *circularis*, develop specialized cells called heterocysts that contain nitrogenase enzymes used for the biocatalytic reduction of atmospheric nitrogen into ammonia [14]. This special ability to fix atmospheric nitrogen makes these cyanobacteria potential producers of fertilizers [6]. In addition, they are capable of producing hydrogen under certain conditions [4,15]. Figures 1(c) and 1(d) show the micrographs of *A. elenkinii* and *circularis*, respectively.

The cyanobacterium *A. elenkinii* consists of spheroidal vegetative cells with 4–5 μm minor diameter and 5–7 μm major diameter and nearly spherical heterocysts 3–4 μm in diameter. By contrast, the cyanobacterium *A. circularis* consists of aspherical vegetative cells and spherical heterocysts about 8–10 μm in diameter. These cells are arranged in a nearly circular ring and number between 10 and 25 cells per ring.

The cultivation of photosynthetic micro-organisms in photobioreactors (PBRs) exposed to sunlight has been studied extensively due to the above-mentioned applications. Photosynthetic micro-organisms absorb photons in the photosynthetically active radiation (PAR) region ranging from 400 to 700 nm thanks to photosynthetic pigments, such as chlorophylls and carotenoids [16]. They also scatter light due to the refractive index mismatch between the cells and the surrounding growth medium [17]. The economic viability of large-scale cultivation can be severely reduced by poor light penetration in dense micro-organism cultures [18]. In order to design and operate PBRs with optimum light availability, it is essential to accurately predict light transfer in the culture [18,19]. To do so, the spectral radiation characteristics of the photosynthetic micro-organisms are necessary. They can be measured experimentally [18,20] or predicted numerically [21–23]. Experimental measurements can faithfully capture the effect of the micro-organisms' size, shape, and polydispersity. However, they require expensive equipment and can be time consuming. Radiation characteristics of spherical photosynthetic micro-organisms can be easily determined from the Lorenz–Mie theory [24]. Similarly, solutions of Maxwell's

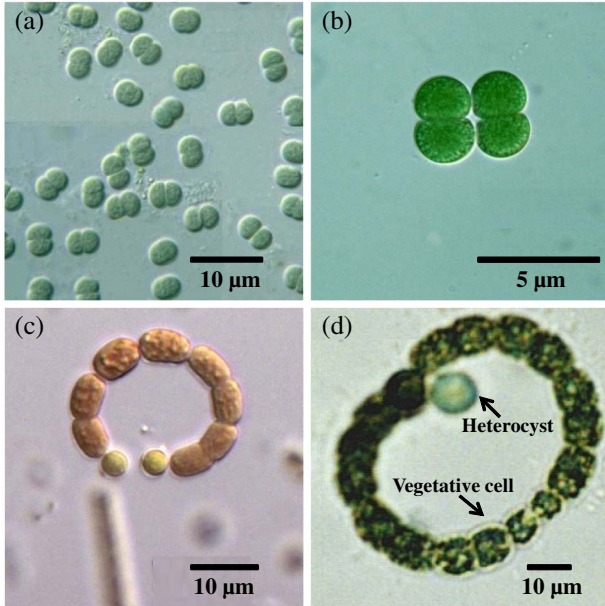


Fig. 1. Micrographs of cyanobacteria: (a) free floating *Synechocystis sp.*, (b) *Synechocystis sp.* immediately after cell division, (c) *Anabaenopsis elenkinii*, and (d) *Anabaenopsis circularis*. Reproduced with permission from (a), (b) Prof. Yuuji Tsukii (Hosei University, <http://protist.i.hosei.ac.jp/>), (c) Dr. Seija Hällfors (University of Jyväskylä Biology Department, <http://www.jyu.fi/bio/kasviplankton/uusin/>), and (d) Dr. Roger Burks (University of California at Riverside), Prof. Mark Schneegurt (Wichita State University), and Cyanosite (<http://www.cyanosite.bio.purdue.edu/>).

equations have also been developed for coated spheres [25] and infinitely long cylinders [26–28]. The radiation characteristics of particles with more complex and irregular shapes can be predicted numerically using (i) the T-matrix method [29–32], (ii) the discrete-dipole approximation [33], and (iii) the finite-difference time-domain method [34], for example. However, numerical predictions can be complicated by the diverse and sometimes complex micro-organism morphology. In addition, their large size compared with the radiation wavelength and their polydispersity require time-consuming and resource-intensive computations [35]. Finally, inverse methods used to retrieve the complex index of refraction and/or the morphology and/or the concentration of the micro-organisms from experimental measurements require numerous iterations of an already time-consuming forward problem [22,36–38].

The present study aims to identify particles of simple shape with radiation characteristics equivalent to those of *Synechocystis sp.*, *A. elenkinii*, and *circularis*, and other micro-organisms with similar morphologies. Such equivalent particle approximations could be computationally advantageous and practical for predicting light transfer in PBRs and for remote sensing applications provided that it can achieve an acceptable degree of accuracy [36,39].

2. BACKGROUND

A. Scattering Matrix

The four Stokes parameters, I , Q , U , and V , forming the Stokes vector, are used to describe an electromagnetic wave in terms of its intensity, degree of polarization, and ellipsometric characteristics [31]. Upon single scattering by a particle of

arbitrary shape and orientation, the Stokes vector of the incident radiation represented by $\mathbf{I}_{\text{inc}}(\hat{s}_i) = (I_{\text{inc}}, Q_{\text{inc}}, U_{\text{inc}}, V_{\text{inc}})^T$, is transformed into the Stokes vector of the scattered radiation at location \mathbf{r} , denoted by $\mathbf{I}_{\text{sca}}(\mathbf{r}, \hat{s}) = (I_{\text{sca}}, Q_{\text{sca}}, U_{\text{sca}}, V_{\text{sca}})^T$. These vectors are related by the 4×4 Mueller matrix $[\mathbf{Z}(\Theta)]$ according to [32]

$$\mathbf{I}_{\text{sca}}(\mathbf{r}, \hat{s}) = \frac{1}{r^2} [\mathbf{Z}(\Theta)] \mathbf{I}_{\text{inc}}(\hat{s}_i), \quad (1)$$

where r is the norm of the location vector \mathbf{r} . The scattering angle, denoted by Θ , corresponds to the angle between the incident and scattered directions, \hat{s}_i and \hat{s} , respectively.

For randomly oriented particles with a plane of symmetry, it is more convenient to use the normalized (or Stokes) scattering matrix $[\mathbf{F}(\Theta)]$ given by [31]

$$[\mathbf{F}(\Theta)] = \frac{4\pi}{C_{\text{sca}}} [\mathbf{Z}(\Theta)], \quad (2)$$

where C_{sca} is the scattering cross section of the particle. When multiplied by the incident monochromatic energy flux, C_{sca} represents the total monochromatic power removed from the incident electromagnetic (EM) wave due to scattering [31]. Similarly, the absorption cross section C_{abs} can be defined such that its product with the incident monochromatic energy flux represents the total monochromatic power absorbed by the particle [31]. The overall extinction of the incident EM wave is due to both absorption and scattering, and the extinction cross section can be defined as $C_{\text{ext}} = C_{\text{abs}} + C_{\text{sca}}$.

The normalized scattering matrix $[\mathbf{F}(\Theta)]$ for a scattering particle with a plane of symmetry is a 4×4 matrix containing eight nonzero elements and six independent elements given by [31,40]

$$[\mathbf{F}(\Theta)] = \begin{bmatrix} F_{11}(\Theta) & F_{12}(\Theta) & 0 & 0 \\ F_{12}(\Theta) & F_{22}(\Theta) & 0 & 0 \\ 0 & 0 & F_{33}(\Theta) & F_{34}(\Theta) \\ 0 & 0 & -F_{34}(\Theta) & F_{44}(\Theta) \end{bmatrix}.$$

The element $F_{11}(\Theta)$ represents the scattering phase function normalized according to [31]

$$\frac{1}{4\pi} \int_{4\pi} F_{11}(\Theta) d\Omega = 1, \quad (3)$$

where Ω is the solid angle around the scattering angle Θ . The asymmetry factor is defined as [41]

$$g = \frac{1}{4\pi} \int_{4\pi} F_{11}(\Theta) \cos \Theta d\Omega. \quad (4)$$

It is equal to 0 for isotropic scattering and -1 and 1 for purely backward and forward scattering, respectively [18]. The ratio $-F_{12}(\Theta)/F_{11}(\Theta)$ represents the degree of linear polarization of the scattered radiation when the particle is exposed to unpolarized incident radiation [42]. The ratio $F_{22}(\Theta)/F_{11}(\Theta)$ can be interpreted as a measure of the particle's deviation from a sphere [42]. The ratio $F_{34}(\Theta)/F_{11}(\Theta)$ indicates the amount of obliquely polarized light at 45° [42]. For spherical scatterers, $F_{22}(\Theta) = F_{11}(\Theta)$ and $F_{33}(\Theta) = F_{44}(\Theta)$ [42].

B. Heterogeneous and Spheroidal Particles

Despite the heterogeneous nature of photosynthetic microorganism cells, they have often been treated as homogeneous with some effective complex index of refraction [17,22,37,43]. This assumption was validated by Quirantes and Bernard [22] who modeled single-cell microalgae as coated spheres or coated spheroids to account for their complex intracellular structures. These coated particles had core to particle volume ratios ranging from 0.4 to 1 and size parameters based on outer diameter up to a maximum value of 30. The outer coating was assumed to be nonabsorbing and represented the cellular cytoplasm. By contrast, the inner core, representing the organelles and chloroplasts, was absorbing and featured a larger refractive index than the outer coating. The authors found that light absorption and scattering efficiency factors of a homogeneous sphere with volume-averaged complex index of refraction were similar to those of the coated sphere [22].

Moreover, Lee *et al.* [37] showed that the radiation characteristics of spheroidal unicellular microalgae were similar to those of spheres with identical surface area provided that their aspect ratio was less than 1.33. These observations suggest that typical micro-organisms' cells, such as those shown in Fig. 1, can be treated as homogeneous spheres with an effective complex index of refraction.

C. Aggregates of Spherical Monomers

The development of the superposition T-matrix method to predict absorption and scattering of electromagnetic waves by multisphere clusters was first motivated by the study of the interaction between radiation and carbonaceous soot particles modeled as aggregates of connected spheres (or monomers) a few nanometers in diameter [30]. It has also been used for a wide variety of applications [44] ranging from plasmon resonance in aggregates of gold [45] and silver [46] nanoparticles to the interpretation of solar radiation scattered by cometary dust [47] and filamentous cyanobacteria [39].

The method is based on the superposition solutions of Maxwell's equations where the EM field scattered by the entire aggregate of monomers is the sum of the EM fields scattered by each of the constituent monomer [48]. The EM field incident onto a monomer takes into account not only the incident EM field but also the scattered fields from all the other monomers of the aggregate [48]. The interacting fields are transformed into a system of sphere-centered equations for the scattering coefficients and inverted to obtain the T-matrix [48]. Using an analytical rotation transformation rule to integrate the incident EM field over every propagation direction and polarization, the scattering (C_{scat}) and extinction (C_{ext}) cross sections and scattering matrix elements of a randomly oriented aggregate of spheres can be obtained from operations on the T-matrix [48].

D. Equivalent Scattering Particles

Several studies have used equivalent particles with simple geometries and some effective complex index of refraction to approximate the radiation characteristics of nonspherical particles and aggregates of spherical monomers. Mengüç *et al.* [49] approximated irregularly shaped pulverized coal particles as volume equivalent spheres in order to retrieve their effective complex index of refraction from experimental radiation

characteristics measurements. The coal particles were assumed to be spherical and their mean diameters were measured using scanning electron microscopy so as to compute their volumes. Liou and Takano [50] compared the absorption and scattering cross sections and asymmetry factor of cubes, hexagonal ice crystals, and irregular convex and concave particles with size parameters larger than 30 with those predicted by Lorenz–Mie theory for their volume or surface area equivalent spheres. The range of complex index of refraction used for the particles was representative of atmospheric particulates, i.e., carbon and water. The authors concluded that nonspherical particles have smaller asymmetry factors than their volume or surface area equivalent spherical counterparts. They also found that volume equivalent spheres had similar absorption cross sections but smaller scattering cross sections than the actual nonspherical particles. Kahnert *et al.* [51] computed the extinction and scattering cross sections, the single-scattering albedo, and the asymmetry factor of ensembles of randomly oriented polyhedral prisms with different number of side facets, aspect ratios, and sizes. The authors compared these radiation characteristics with those of ensembles comprising solely of spheres, spheroids, or finite-length cylinders with the same complex index of refraction and identical volume or surface area distribution. They found that the best approximation was achieved using ensembles of volume equivalent spheres. Yang *et al.* [52] approximated various platonic particles as equivalent spheres with identical (i) geometric dimension, (ii) surface area, (iii) volume, or (iv) volume-to-surface area ratio. The authors found that the volume equivalent spheres offered the best approximation for the extinction efficiency factor, single-scattering albedo, and scattering matrix elements of platonic particles. However, all these approximations still resulted in significant errors. In addition, the authors recommended that the absorption and scattering cross sections should be used instead of the efficiency factors due to the difference of geometric cross sections between the platonic particles and the equivalent spheres. Gordon [43] showed that approximating finite cylinders as volume equivalent spheres resulted in large errors in the scattering efficiency factor but good agreement in the absorption efficiency factor.

Latimer [53] experimentally measured the extinction coefficients at 474 nm of randomly oriented fractal aggregates of 2 to 128 spherical latex particles in water. The author found that the aggregates could be approximated as coated spheres whose core and shell had the same complex index of refraction as water and latex, respectively. The volume of the coating was taken as the total volume of the latex particles constituting the aggregates while the volume of the core was taken as that of “the spaces between the particles” derived from fractal theory. While Latimer's results showed good agreement between the radiation measurements of the latex particles and the theoretical predictions for the equivalent coated spheres, his choice of using only five discrete bins to represent the entire monomer size distribution may have introduced significant errors. Tien and Drolen [54] computed the absorption and scattering cross sections of soot aggregates consisting of 2 to 136 spherical monodisperse monomers with size parameter ranging from 0.05 to 0.2, refractive index ranging from 1.5 to 2.2, and absorption index ranging from 0 to 2.6. These monomers were aggregated either in

straight chains or spheroidal, ellipsoidal, or cube-like clusters. They found that a volume equivalent sphere with the same complex index of refraction as the monomers gave similar absorption and scattering cross sections as the soot aggregate. Recently, Lee and Pilon [39] showed that the absorption and scattering cross sections per unit length and asymmetry factor of randomly oriented linear chains of optically soft spheres with size parameter ranging from 0.01 to 10, could be approximated as that of randomly oriented, volume equivalent, and infinitely long cylinders provided that the number of spheres in the chain was sufficiently large. However, this approximation was not valid for the scattering matrix elements.

Light transfer in homogeneous absorbing, scattering, and nonemitting micro-organism suspensions, such as those found in PBRs, is governed by the radiative transfer equation (RTE) [18]. In PBRs, the micro-organisms are typically uniformly distributed and randomly oriented thanks to bubble sparging or stirring, for example [55]. The absorption and scattering cross sections as well as the scattering phase function of these randomly oriented micro-organisms are necessary input parameters to solve the RTE [18]. Unfortunately, cyanobacteria, such as those shown in Fig. 1, have very complex morphologies and large size parameters. Accurately predicting their radiation characteristics would require large amounts of time and computational resources. Therefore, the present study aims to demonstrate that photosynthetic micro-organisms, such as those shown in Fig. 1, can be approximated by some equivalent particle with a simple geometry. The effects of the cells' complex index of refraction and polydispersity were also investigated.

3. ANALYSIS

A. Problem Statement

First, actual cyanobacteria shown in Fig. 1 were represented by idealized aggregates of optically soft and homogeneous spherical monomers. Figure 2(a) shows a bisphere consisting of two identical adjoining spheres of radius r_s representing the dumbbell-shape of *Synechocystis sp.* cells [Fig. 1(a)]. Similarly, Fig. 2(b) shows a quadisphere modeling the morphology of *Synechocystis sp.* cells immediately after cell division [Fig. 1(b)]. Finally, Figs. 2(c) and 2(d) show circular rings of spheres with an arbitrary number N_s of monomers representing filamentous cyanobacteria, such as *A. elenkinii* and *A. circularis* [Figs. 1(c) and 1(d)].

Let us consider randomly oriented bispheres, quadispheres, and circular rings of spheres consisting of N_s monodisperse spherical monomers of radius r_s and complex index of refraction $m_s = n_s + ik_s$, where n_s and k_s are the refractive and absorption indices, respectively. The surrounding medium was assumed to be nonabsorbing with refraction index $m_m = n_m$. The relative complex index of refraction of the monomers can be defined as $m = n + ik = m_s/n_m$. The size parameter of the monomers constituting the bispheres, quadispheres, and rings of spheres was defined as $\chi_s = 2\pi r_s/\lambda$, where λ is the wavelength of the incident radiation. In general, the radiation characteristics of bispheres, quadispheres, and rings of spheres depend on (i) the aggregate morphology, (ii) the relative complex refraction index m , and (iii) the monomer number N_s and size parameter χ_s .

Previous studies [39,43,50,51,54] indicate that the equivalent particle should have the same volume as the aggregate

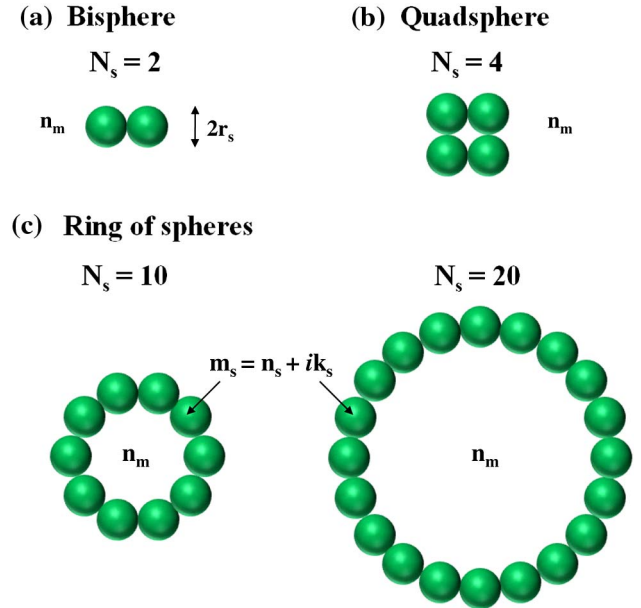


Fig. 2. Schematic of simulated (a) bispheres, (b) quadispheres, and (c) rings of spheres with $N_s = 5$ and 10 monodisperse monomers of radius r_s and complex index of refraction $m_s = n_s + ik_s$ surrounded by a nonabsorbing medium of refraction index n_m . These idealized aggregates are representative of the cyanobacteria shown in Fig. 1.

to match their absorption cross sections. This can be attributed to the fact that absorption is a volumetric phenomenon. On the other hand, scattering is due in part to the complex index of refraction mismatch across the interface between the aggregates' monomers and the surrounding medium. Thus, an equivalent particle with the same surface area as the aggregate could also have similar scattering cross sections. Alternatively, the projected area is directly proportional to the amount of energy incident on the aggregates for a given aggregate orientation. Hence, matching the average projected area of the equivalent particle with that of the randomly oriented aggregate offers another alternative. The most common approach is to approximate a particle of complex shape or an aggregate of spherical monomers as an equivalent sphere [43,51,52]. However, a sphere is defined by a single geometric parameter: its radius. Thus, the equivalent sphere can only match either the volume, the surface area, or the average projected area of the aggregate. On the other hand, a coated sphere is defined by its inner and outer radii. Both can be adjusted to match two geometric characteristics of the aggregates, such as its volume and its surface area or its volume and its average projected area.

In order to determine the best equivalent particle, the absorption and scattering cross sections as well as the scattering matrix elements of the different possible equivalent spheres or coated spheres will be compared systematically with predictions by the superposition T-matrix method for randomly oriented bispheres, quadispheres, and rings of spheres. The monomers had size parameter χ_s ranging from 0.01 to 10, refractive index n_s varying between 1.37 and 2, and absorption index k_s from 0.0053 to 0.133. The surrounding medium was nonabsorbing with refractive index $n_m = 1.33$. These values were representative of cyanobacteria suspended in growth medium and exposed to sunlight. The wavelength of incident light was taken as 676 nm corresponding to the absorption

peak of chlorophyll *a* [16]. Finally, the inner core of the equivalent coated sphere was assumed to have the same refractive index n_m as the surrounding medium while the coating and the equivalent sphere were assumed to have the same complex index of refraction $m_s = n_s + ik_s$ as the monomers.

B. Methodology

1. Geometric Consideration

The radius $r_{v,eq}$ of the volume equivalent sphere with the same volume as that of an aggregate consisting of N_s monomers of radius r_s can be expressed as

$$r_{v,eq} = r_s \sqrt[3]{N_s}. \quad (5)$$

Similarly, the surface area and volume of coated spheres of outer $r_{s,eq,o}$ and inner $r_{s,eq,i}$ radii are equal to $4\pi r_{s,eq,o}^2$ and $4\pi(r_{s,eq,o}^3 - r_{s,eq,i}^3)/3$, respectively. Thus, the volume and surface area equivalent coated sphere, featuring the same volume and surface area as the aggregate, is such that $r_{s,eq,o}$ and $r_{s,eq,i}$ are given by

$$r_{s,eq,o} = r_s \sqrt{N_s} \quad \text{and} \quad r_{s,eq,i} = r_s \sqrt[3]{N_s^{3/2} - N_s}. \quad (6)$$

Similarly, the outer $r_{\bar{A}_p,eq,o}$ and inner $r_{\bar{A}_p,eq,i}$ radii of the equivalent coated sphere with identical volume and average projected area \bar{A}_p as the randomly oriented aggregate can be written as

$$r_{\bar{A}_p,eq,o} = \sqrt{\frac{\bar{A}_p}{\pi}} \quad \text{and} \quad r_{\bar{A}_p,eq,i} = \sqrt[3]{\left(\frac{\bar{A}_p}{\pi}\right)^{3/2} - N_s r_s^3}. \quad (7)$$

A priori, the average projected area \bar{A}_p depends on the number N_s and radius r_s of monomers in the aggregate. Figure 3 illustrates the projected area of a bisphere on the x - y plane when viewed along the z -axis. For a given orientation, the projected area $A_{p,b}$ of a bisphere is represented by the area enclosed by two intersecting circles and is given by

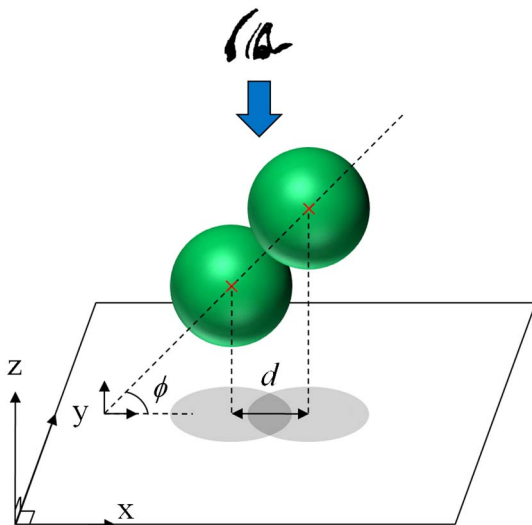


Fig. 3. Schematic of the projected area of a bisphere onto the x - y plane when viewed along the z -axis.

$$A_{p,b}(r_s, d) = 2\pi r_s^2 - 2r_s^2 \cos^{-1}\left(\frac{d}{2r_s}\right) + \frac{1}{2}d\sqrt{4r_s^2 - d^2}, \quad (8)$$

where d is the distance between the centers of the two projected discs. This distance is given by $d = 2r_s \cos \phi$, where ϕ is the angle between the longitudinal axis of the bisphere and the x - y plane. For example, when the bisphere is viewed along its longitudinal axis, $\phi = \pi/2$ or $-\pi/2$. Then, the distance d between the two projected circles is zero and the projected area $A_{p,b}$ is equal to that of a single sphere πr_s^2 , as predicted by Eq. (8). As bispheres are axisymmetric, the average projected area of a bisphere $\bar{A}_{p,b}$ can be obtained by integrating the expression in Eq. (8) with respect to ϕ between $-\pi/2$ and $\pi/2$ to yield

$$\bar{A}_{p,b} = \frac{1}{\pi} \int_{-\pi/2}^{\pi/2} A_{p,b}(r_s, \phi) d\phi \approx 5.35r_s^2. \quad (9)$$

For aggregates with more than two monomers, the average projected area can be calculated numerically by (i) fixing the position of the observer, (ii) rotating the aggregate through numerous orientations around its geometric center, and (iii) computing the different projected area before averaging. The code implementing this procedure was developed and successfully validated with the above expression of $\bar{A}_{p,b}$ for bispheres. For quadspheres and rings of N_s spheres, the average projected area \bar{A}_p was found to be proportional to the square of the monomer radius r_s such that

$$\bar{A}_p = \alpha(N_s)r_s^2, \quad (10)$$

where α is a constant depending on the number of monomers N_s in the aggregate. For quadspheres, $\alpha(4)$ was found to be equal to 9.70 while for a circular ring of N_s monodisperse monomers, $\alpha(N_s)$ was such that $\alpha(N_s) = 2.42N_s$ for $N_s \geq 5$. In practice, \bar{A}_p can be measured using image analysis of two-dimensional micrographs of freely suspended microorganisms [56].

2. Radiation Characteristics

The absorption $\langle Q_{abs} \rangle$ and scattering $\langle Q_{sca} \rangle$ efficiency factors and the normalized Stokes scattering matrix elements of randomly oriented bispheres, quadspheres, and rings of monodisperse spheres of radius r_s were computed using the superposition T-matrix code described in [57]. On the other hand, the absorption and scattering efficiency factors and the scattering matrix elements of the different equivalent homogeneous spheres and coated spheres were computed based on Lorenz-Mie theory [24,25,58]. The Matlab codes implementing these solutions were obtained from [58].

The absorption $\langle C_{abs}^a \rangle$ and scattering $\langle C_{sca}^a \rangle$ cross sections of the randomly oriented aggregates were estimated from the numerically predicted absorption $\langle Q_{abs}^a \rangle$ and scattering $\langle Q_{sca}^a \rangle$ efficiency factors according to

$$\langle C_{abs}^a \rangle = \langle Q_{abs}^a \rangle \pi r_{v,eq}^2 \quad \text{and} \quad \langle C_{sca}^a \rangle = \langle Q_{sca}^a \rangle \pi r_{v,eq}^2, \quad (11)$$

where $r_{v,eq}$ is the radius of the volume equivalent sphere given by Eq. (5) and $\pi r_{v,eq}^2$ represents its projected surface area [57]. Similarly, the cross sections of the volume equivalent sphere were obtained according to $C_{abs/sca}^s = Q_{abs/sca}^s \pi r_{v,eq}^2$. In the

case of the volume and surface area equivalent coated spheres, the cross sections were estimated based on the outer radius, i.e., $C_{\text{abs}/\text{sca},V+S}^{\text{cs}} = Q_{\text{abs}/\text{sca},V+S}^{\text{cs}} \pi r_{s,\text{eq},o}^2$. Finally, the cross sections of the volume and average projected area equivalent coated sphere were computed based on the average projected area of the aggregates such that $C_{\text{abs}/\text{sca},V+\bar{A}_p}^{\text{cs}} = Q_{\text{abs}/\text{sca},V+\bar{A}_p}^{\text{cs}} \bar{A}_p$.

Finally, the relative errors in the absorption and scattering cross sections and asymmetry factors between the bispheres, quadspheres, and rings of spheres and their equivalent spheres and coated spheres were used to identify the best approximation.

4. RESULTS AND DISCUSSION

A. Absorption and Scattering Cross Sections

Figure 4 shows the absorption cross section $\langle C_{\text{abs}}^a \rangle$ of randomly oriented (a) bispheres and quadspheres, and (b) circular rings of 10 and 20 spheres as a function of monomer size parameters χ_s ranging from 0.01 to 10. Here, the relative complex index of refraction of the monomers was taken as $m = 1.03 + i0.004$ representative of photosynthetic microorganisms in their growth medium exposed to light in the PAR region [37,43]. They also plot the absorption cross section of the corresponding equivalent spheres and coated spheres. Figures 4(a) and 4(b) indicate that the absorption cross section increased with increasing number of monomers N_s and size parameter χ_s . They also established that $\langle C_{\text{abs}}^a \rangle$

was linearly proportional to χ_s^3 . In addition, Figs. 4(c) to 4(f) show the relative errors in the absorption cross section between the aggregates considered and the different equivalent particles as functions of χ_s . As observed in the literature [39,43,50,51], all equivalent spheres and coated spheres featured very similar absorption cross sections. The relative error in the absorption cross sections of the bispheres and quadspheres was less than 1.5% for all equivalent particles and size parameter χ_s considered. Similarly, the relative error in the absorption cross sections of the rings of 10 and 20 spheres and of the equivalent particles was less than 7%. Such good agreement can be attributed to the fact that all equivalent spheres and the shell of the equivalent coated spheres had the same volume as that of the bispheres, quadspheres, and rings of spheres for any given value of χ_s . These observations indicate that self-shading in these aggregates had negligible effect on the absorption cross sections thanks to the relatively small monomer absorption index $k_s = 0.0053$. Overall, the volume and average projected area equivalent coated spheres provided the best approximation of the absorption cross section for all values of χ_s . In fact, the corresponding relative error between the superposition T-matrix prediction and this approximation did not exceed 1% for all aggregates considered.

Figure 5 shows the scattering cross section $\langle C_{\text{sca}}^a \rangle$ of randomly oriented (a) bispheres and quadspheres and (b) circular rings of 10 and 20 spheres as a function of χ_s for

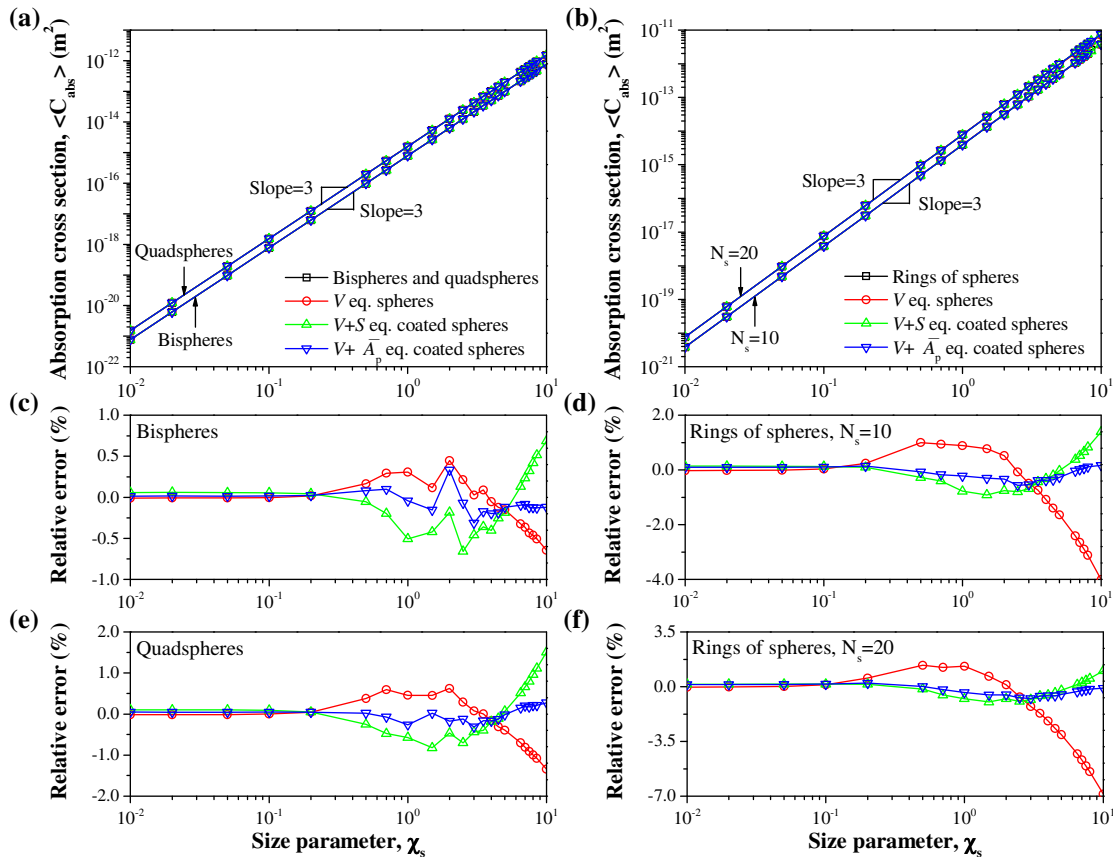


Fig. 4. Absorption cross section of randomly oriented (a) bispheres and quadspheres and (b) rings of $N_s = 10$ and 20 spheres and of their corresponding equivalent spheres and coated spheres as a function of monomer size parameter χ_s ranging from 0.01 to 10 for $m = 1.03 + i0.004$. Relative errors in the absorption cross section between the T-matrix predictions and the equivalent particles for (c) bispheres, (e) quadspheres, (d) rings of 10 spheres, and (f) rings of 20 spheres.

$m = 1.03 + i0.004$. They also plot the scattering cross section of the corresponding equivalent spheres or coated spheres. Here also, the scattering cross sections of the aggregates were found to increase with increasing monomer size parameters χ_s and number of monomers N_s . For χ_s less than 0.1, the scattering cross section was directly proportional to χ_s^6 for all aggregates considered. Figures 5(c)–5(f) show the relative errors in scattering cross sections resulting between predictions from the superposition T-matrix and the different equivalent particle approximations. The relative errors in the scattering cross sections for all the equivalent particles were found to be less than 5% when χ_s was smaller than 0.1. In this case, the particles were much smaller than the wavelength of the incident EM wave. Each volume element in the aggregate or the equivalent scattering particle scattered light independently of the others [27]. Note that the range of χ_s for which good agreement was observed was smaller for the rings of 10 and 20 spheres because they had larger total volume for the same value of χ_s . As χ_s increased, the size of the aggregate became comparable to the wavelength of the incident EM wave and the relative errors in the scattering cross sections increased. For χ_s larger than 1, the relative errors in the scattering cross section between the T-matrix predictions and the volume equivalent spheres and the volume and surface area equivalent coated spheres were excessively large. By contrast, the relative errors corresponding to the volume and average

projected area equivalent coated spheres was less than 6%. Thus, both the volume and the average projected area of the aggregate should be preserved by the equivalent particle in order to match the absorption and scattering cross sections. Again, this cannot be achieved by an equivalent sphere.

Figure 6(a) shows $\langle C_{\text{abs}}^a \rangle$ as a function of the product $N_s \chi_s^3$ for bispheres, quadspheres, and rings of 10 and 20 spheres. First, it is interesting to note that the data for $\langle C_{\text{abs}}^a \rangle$ for the four types of aggregates collapsed onto a single line. In fact, for all these aggregates, $\langle C_{\text{abs}}^a \rangle$ was linearly proportional to $N_s \chi_s^3$ for all monomers size parameters χ_s considered. Similarly, Fig. 6(b) shows $\langle C_{\text{sca}}^a \rangle$ as a function of the product $N_s^2 \chi_s^6$ for bispheres, quadspheres, and rings of 10 and 20 spheres. It indicates that the data for these different aggregates collapsed also onto a single line and that $\langle C_{\text{sca}}^a \rangle$ was proportional to $N_s^2 \chi_s^6$ for $\chi_s \leq 0.1$. These observations are consistent with predictions by the Rayleigh–Debye–Gans approximation valid for fractal aggregates of small and optically soft monomers, i.e., $\chi_s \ll 1$ and $|m - 1| \ll 1$ [59].

Overall, approximating bispheres, quadspheres, and rings of spheres by equivalent coated spheres with identical volume and average projected area provided the best estimates of $\langle C_{\text{abs}}^a \rangle$ and $\langle C_{\text{sca}}^a \rangle$ for the four types of aggregates of interest for all monomer size parameters χ_s and number of monomers N_s considered. Thus, other equivalent particles will not be considered further.

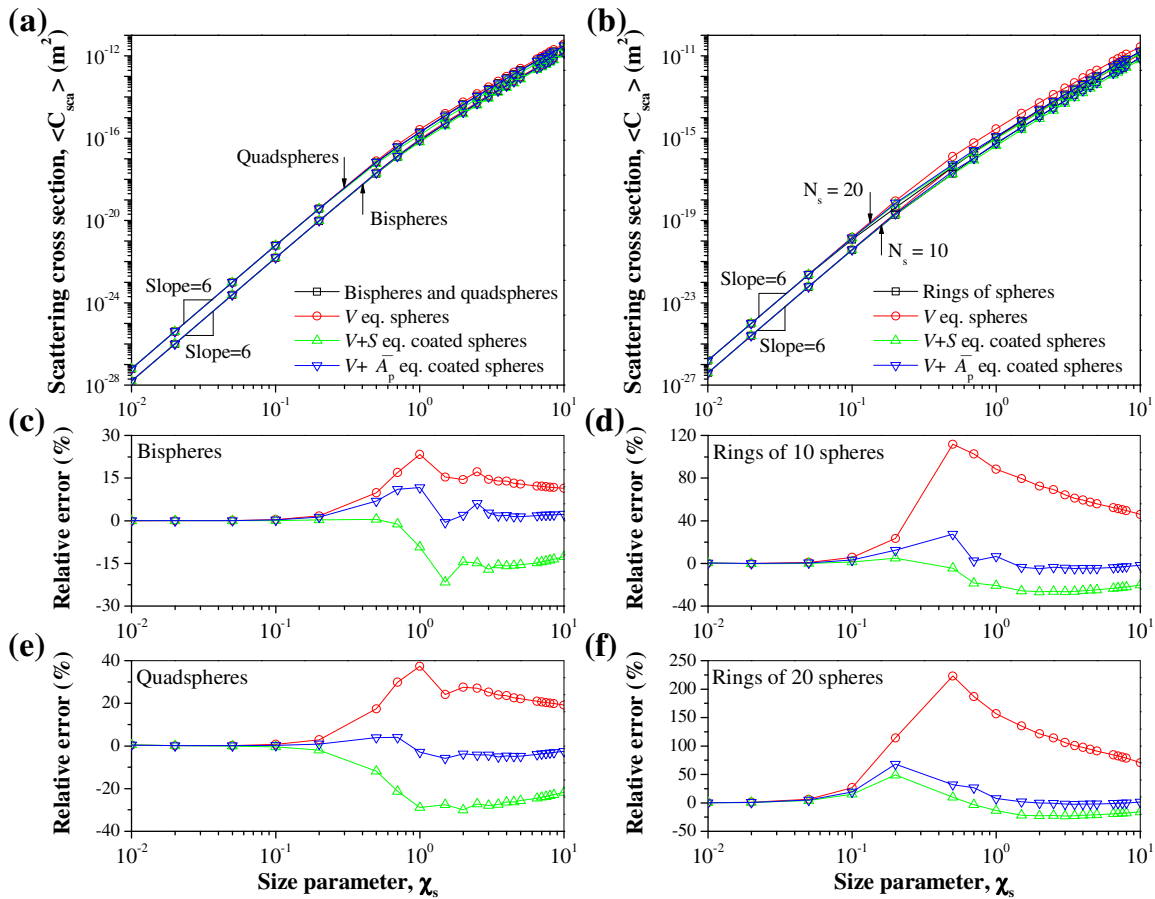


Fig. 5. Scattering cross section of randomly oriented (a) bispheres and quadspheres and (b) rings of $N_s = 10$ and 20 spheres and of their corresponding equivalent spheres and coated spheres as a function of monomer size parameter χ_s ranging from 0.01 to 10 for $m = 1.03 + i0.004$. Relative errors in the scattering cross sections between the T-matrix predictions and the equivalent particles for (c) bispheres, (e) quadspheres, (d) rings of 10 spheres, and (f) rings of 20 spheres.

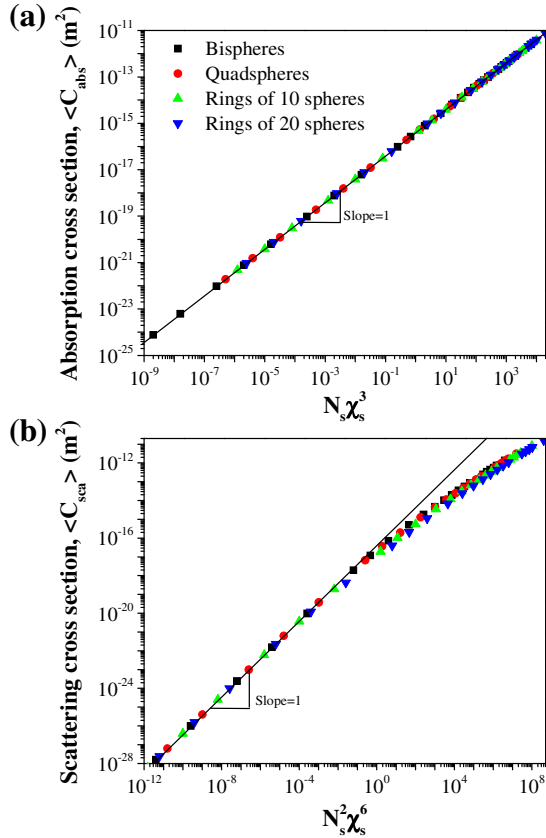


Fig. 6. (a) Absorption and (b) scattering cross sections of bispheres, quadspheres, rings of 10 and 20 spheres as functions of $N_s \chi_s^3$ and $N_s^2 \chi_s^6$, respectively.

B. Scattering Phase Function and Asymmetry Factor

Figure 7 shows the scattering phase function $F_{11}(\Theta)$ of randomly oriented (a) bispheres, (b) quadspheres, and circular rings of (c) 10 and (d) 20 spheres as functions of the scattering angles Θ for monomer size parameters $\chi_s = 0.01, 0.1, 1, \text{ and } 10$ and for $m = 1.03 + i0.004$. It also plots the phase function of the corresponding volume and average projected area equivalent coated spheres. For any aggregate with monomer size parameter χ_s between 0.01 and 0.1, the phase function was nearly uniform in all directions, corresponding to quasi-isotropic scattering. For monomer size parameter χ_s equal to 1 and 10, scattering was mainly and increasingly in the forward direction. In addition, $F_{11}(\Theta)$ oscillated strongly with scattering angle Θ for χ_s equal to 10. The number of oscillation lobes increased with increasing number of monomers N_s and with size parameter χ_s . The resonance angles and amplitudes of these oscillations were different for bispheres, quadspheres, and rings of spheres. Note that in practical applications, monomers and aggregates may be polydisperse in terms of size parameter χ_s and monomer number N_s . In this case, we anticipate that the oscillations observed in Fig. 7 would be “washed” out [32]. Moreover, the phase functions of the volume and average projected area equivalent coated spheres showed similar trends as those of the bispheres, quadspheres, and rings of spheres. Very good agreement was systematically observed for bispheres, quadspheres, and rings of spheres monomer size parameter χ_s less than 0.1. However, for χ_s larger than (i) 10 for bispheres and (ii) 1 for quadspheres and rings of spheres, the scattering phase function $F_{11}(\Theta)$

of the equivalent coated spheres featured more oscillations than that of the corresponding aggregate. This could be explained by the fact that the coating behaves as a waveguide causing radiation entering the coating to circumnavigate the core due to total internal refraction [26]. As this guided radiation escapes the coating, it interferes with the reflected radiation to cause the oscillations observed in the phase function of the equivalent coated sphere [26]. Note, however, that for all aggregates and size parameters considered, $F_{11}(0^\circ)$ was predicted within 16%.

Figure 8 shows the asymmetry factor g , defined by Eq. (4), as a function of the monomer size parameter χ_s for (a) bispheres, (b) quadspheres, and circular rings consisting of (c) $N_s = 10$ and (d) 20 spheres, respectively for $m = 1.03 + i0.004$. It also plots the values of g for the corresponding volume and average projected area equivalent coated spheres. The asymmetry factor g was smaller than 0.1 for all aggregates with monomer size parameter χ_s smaller than 0.1. In this regime, the aggregates scattered light quasi-isotropically and feature similar phase functions (Fig. 7). For size parameter larger than 2, the aggregates were largely forward scattering and g approached unity. The asymmetry factor predicted for the volume and average projected area equivalent coated spheres was in good agreement with predictions by the T-matrix method for bispheres and quadspheres for all values of χ_s considered. Good agreement was also found for rings of spheres with size parameter less than 0.1 or larger than 2. The relative error increased with increasing number of monomers N_s present in the ring.

Overall, the asymmetry factor g of the bispheres, quadspheres, and rings of spheres and that of their corresponding volume and average projected area equivalent coated spheres showed reasonably good agreement. Note that knowing the integral radiation characteristics (C_{abs}^a), (C_{sca}^a), and g or the backscattering ratio is sufficient to predict light transfer through a micro-organism suspension contained in open ponds and flat-plate PBRs [21,23]. Thus, in the context of photobioreactor design and control, the above results establish that the types of cyanobacteria shown in Fig. 1 can be approximated as coated spheres with the same volume and projected area and complex indices of refraction of the core and coating equal to those of the medium and cells, respectively.

C. Scattering Matrix Elements

The scattering matrix elements can provide useful information in applications considering the polarization of scattered radiation, such as remote sensing of phytoplankton suspensions [17]. Figures 9(a) to 9(f) show the scattering matrix element ratios $-F_{12}(\Theta)/F_{11}(\Theta)$, $F_{33}(\Theta)/F_{11}(\Theta)$, $F_{44}(\Theta)/F_{11}(\Theta)$, and $F_{34}(\Theta)/F_{11}(\Theta)$ for randomly oriented bispheres and quadspheres as functions of scattering angles Θ for monomer size parameters $\chi_s = 0.01, 0.1, 1, \text{ and } 10$ with $m = 1.03 + i0.004$. They also show the scattering matrix elements of the corresponding volume and average projected area equivalent coated spheres. Similarly, Figs. 10(a)–10(f) show the scattering matrix element ratios for randomly oriented rings of 10 and 20 spheres and their corresponding volume and average projected area equivalent coated spheres. First, the scattering matrix ratio $F_{22}(\Theta)/F_{11}(\Theta)$ was found to be nearly 100% for bispheres, quadspheres, and rings of spheres for all scattering angles Θ between 0 and 180° and

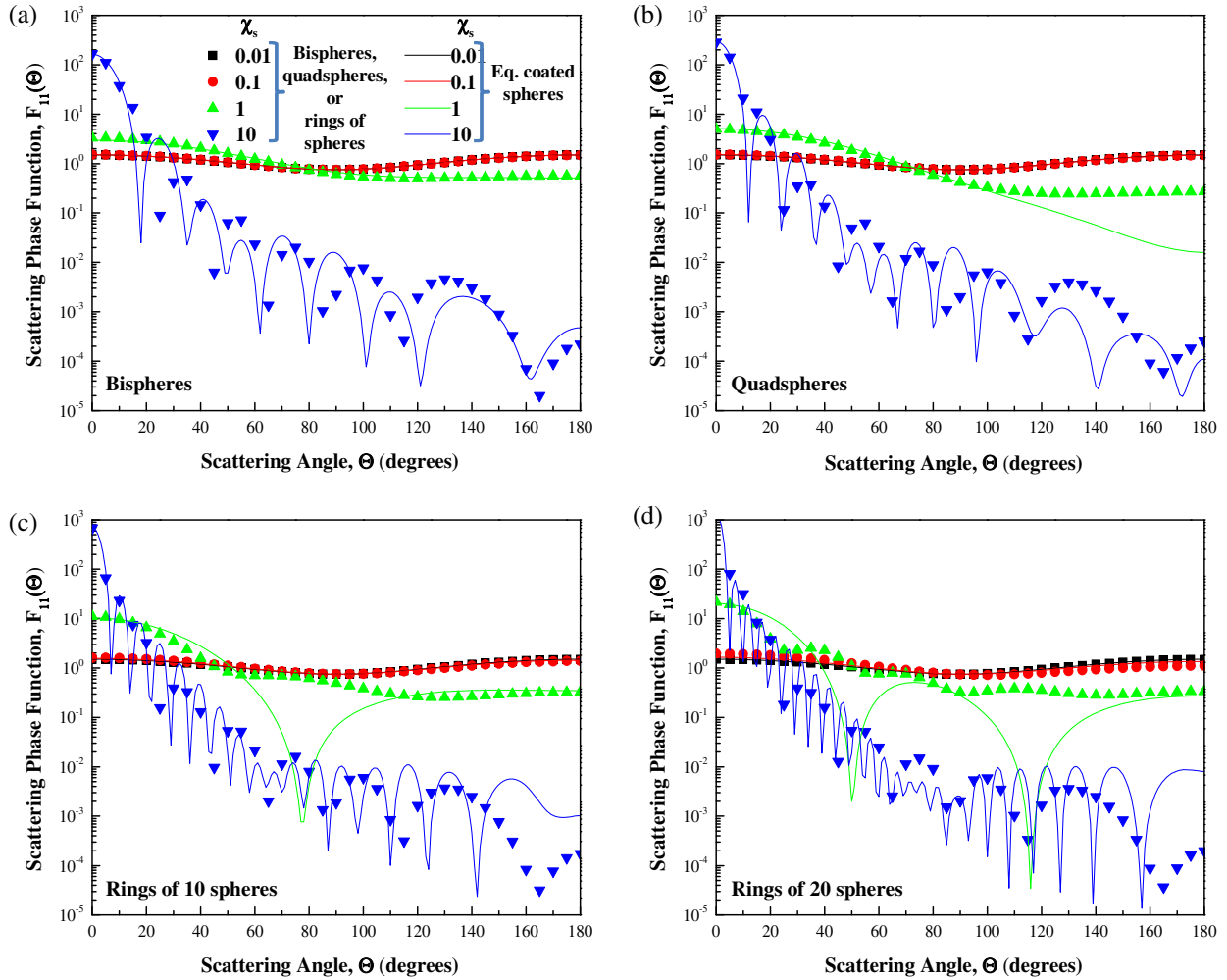


Fig. 7. Scattering phase function $F_{11}(\Theta)$ as a function of scattering angles Θ for (a) bispheres, (b) quadspheres, and rings of spheres with (c) $N_s = 10$ and (d) $N_s = 20$ monomers with monomer size parameters $\chi_s = 0.01, 0.1, 1,$ and 10 and $m = 1.03 + i0.004$ along with those for their corresponding volume and average projected area equivalent coated spheres.

for all size parameters considered (not shown). In addition, for all aggregates, the degree of linear polarization of the scattered radiation, represented by the ratio $-F_{12}(\Theta)/F_{11}(\Theta)$, was zero in the forward ($\Theta = 0^\circ$) and backward ($\Theta = 180^\circ$) directions and reached a maximum of 100% at $\Theta = 90^\circ$. In addition, the element ratios $F_{33}(\Theta)/F_{11}(\Theta)$ and $F_{44}(\Theta)/F_{11}(\Theta)$ of the different aggregates were identical. These results were analogous to those for a single sphere and can be attributed to the dominant role of single scattering by the monomers [60,61]. Indeed, in the case of a single sphere, $F_{22}(\Theta) = F_{11}(\Theta)$ and $F_{33}(\Theta) = F_{44}(\Theta)$.

Oscillations in the scattering matrix element ratios $F_{33}(\Theta)/F_{11}(\Theta)$ and $F_{44}(\Theta)/F_{11}(\Theta)$ appeared for bispheres, quadspheres with size parameter $\chi_s = 10$, and for the circular rings of 10 and 20 spheres with size parameter $\chi_s = 1$ and 10. These oscillations were observed at the same resonance angles as those of the scattering phase function $F_{11}(\Theta)$ shown in Fig. 7. Similarly, $F_{34}(\Theta)/F_{11}(\Theta)$ was equal to zero for all scattering angles for all monomer size parameters except for $\chi_s = 10$ for bispheres and quadspheres and $\chi_s = 1$ and 10 for rings of 10 and 20 monomers. Although the general trends of the scattering matrix element ratios for bispheres, quadspheres, and rings of spheres were captured by those of the

corresponding volume and average projected area equivalent coated sphere, the latter generally exhibited more oscillations for a given value of χ_s . This can also be attributed to the waveguiding effects of the coating previously discussed.

Overall, the volume and average projected area equivalent coated sphere had scattering matrix elements similar to those of the bispheres, quadspheres, and rings of spheres except when χ_s and/or N_s were large. Then, the approximation could not capture the oscillations peaks in $F_{12}(\Theta)/F_{11}(\Theta)$, $F_{22}(\Theta)/F_{11}(\Theta)$, $F_{33}(\Theta)/F_{11}(\Theta)$, $F_{34}(\Theta)/F_{11}(\Theta)$, and $F_{44}(\Theta)/F_{11}(\Theta)$. Therefore, they should not be used for estimating these scattering matrix element ratios.

D. Effect of the Relative Complex Index of Refraction

The volume and average projected area equivalent coated spheres were shown to accurately approximate the absorption and scattering cross sections and asymmetry factor of randomly oriented bispheres, quadspheres, and rings of 10 and 20 spheres consisting of optically soft monomers having relative complex index of refraction $m = 1.03 + i0.004$. One may wonder if this approximation is also valid for aggregates with different refractive and absorption indices. To address this question, the relative refractive index n of the monomers

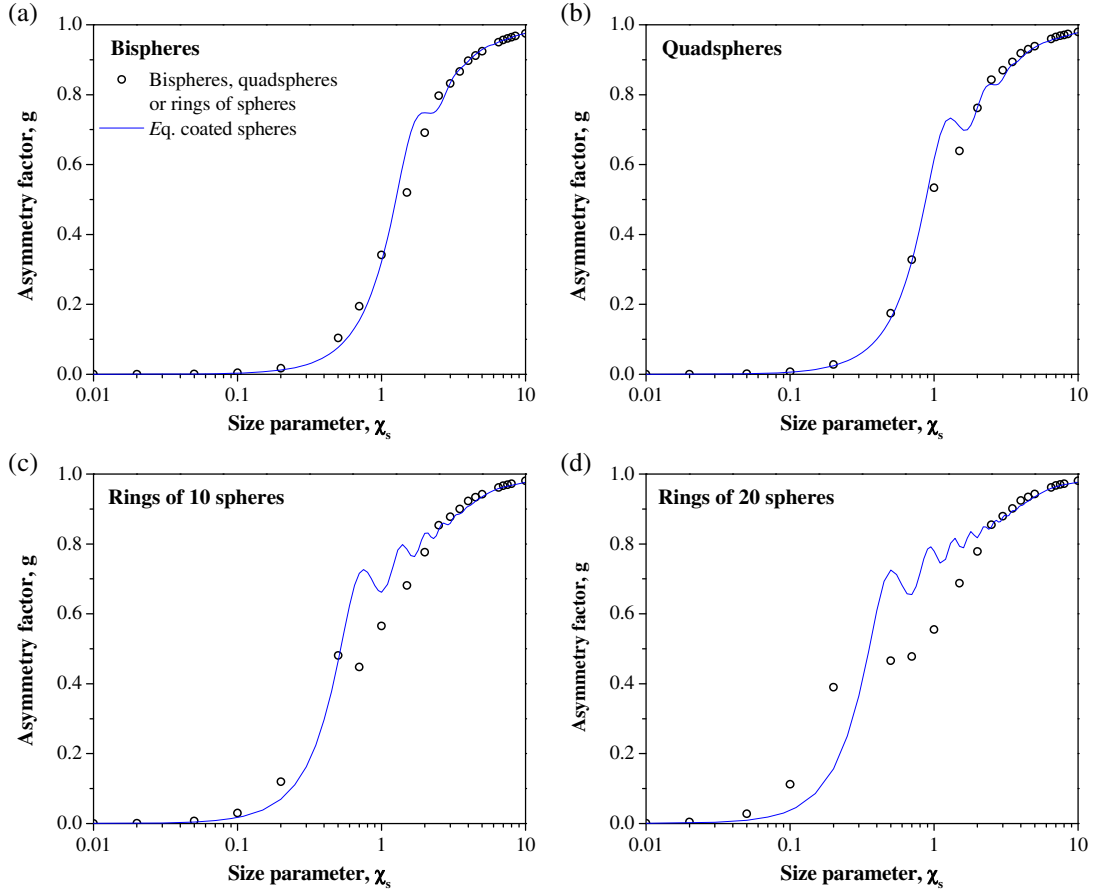


Fig. 8. Asymmetry factor g as a function of monomer size parameter χ_s ranging from 0.01 to 10 with $m = 1.03 + i0.004$ for (a) bispheres, (b) quadspheres, and rings of spheres with (c) $N_s = 10$ and (d) $N_s = 20$ monomers and for their corresponding equivalent volume and average projected area coated spheres.

was increased from 1.03 to 1.2 and 1.5 while keeping the relative absorption index constant and equal to 0.004. Similarly, the relative absorption index k of the monomers was increased from 0.004 to 0.01 and 0.1 while keeping the relative refractive index constant at $n = 1.03$.

Figure 11 shows the absorption [Figs. 11(a)–11(d)] and scattering cross sections [Figs. 11(e)–11(h)] and asymmetry factor [Figs. 11(i)–11(l)] of randomly oriented bispheres, quadspheres, circular rings of 10 and 20 monomers predicted by the T-matrix method as functions of the monomers' size parameters χ_s ranging from 0.01 to 10 for different values of the complex index of refraction. It also plots predictions for the associated corresponding volume and average projected area equivalent coated spheres. It is evident that increasing the relative refractive index n resulted in increasing scattering cross section of bispheres, quadspheres, and rings of spheres due to the larger index mismatch at the interface between the monomers and the surrounding medium. Similarly, increasing the relative absorption index k of the monomers resulted in increasing absorption cross section of all the aggregates considered. For all values of n and k considered, $\langle C_{\text{abs}}^a \rangle$ was proportional to $N_s \chi_s^3$, for all χ_s , and $\langle C_{\text{sca}}^a \rangle$ was proportional to $N_s \chi_s^6$, for χ_s less than 1.0.

The relative error between the absorption cross sections of the aggregates and that of the corresponding volume and average projected area equivalent coated spheres with relative refractive index n equal to 1.2 was less than 8% for all values of

χ_s considered. However, it was significantly larger for $n = 1.5$, particularly for the rings of spheres with increasing size parameter χ_s and number of monomers N_s . On the other hand, increasing the relative absorption index k from 0.004 to 0.1 while n was kept constant at $n = 1.03$ did not affect the performance of the volume and average projected area equivalent coated sphere approximation. Then, the relative errors in the absorption cross section were less than 6% for all values of k and χ_s considered. This indicates that potential shading among monomers was captured by the equivalent coated sphere approximation. These observations are consistent with the literature [39,43,50,51,54]. However, they are valid for optically soft scattering particles such that the penetration depth of the incident EM wave is larger than the particle size. In cases when the size of the scattering particle is larger than the penetration depth, absorption becomes a surface phenomenon and the proposed equivalent coated sphere approximation may not be valid.

Moreover, the relative error in the scattering cross section between the aggregates and their volume and average projected area equivalent coated spheres increased with increasing relative refractive index n and number of monomers N_s in the aggregates. Indeed, scattering is sensitive to particle shape and size and to the mismatch in refractive index between the particle and its surroundings. By contrast, the relative absorption index k did not affect the predictions of $\langle C_{\text{sca}}^a \rangle$ significantly. Here, the same trends in $\langle C_{\text{sca}}^a \rangle$ as those observed in

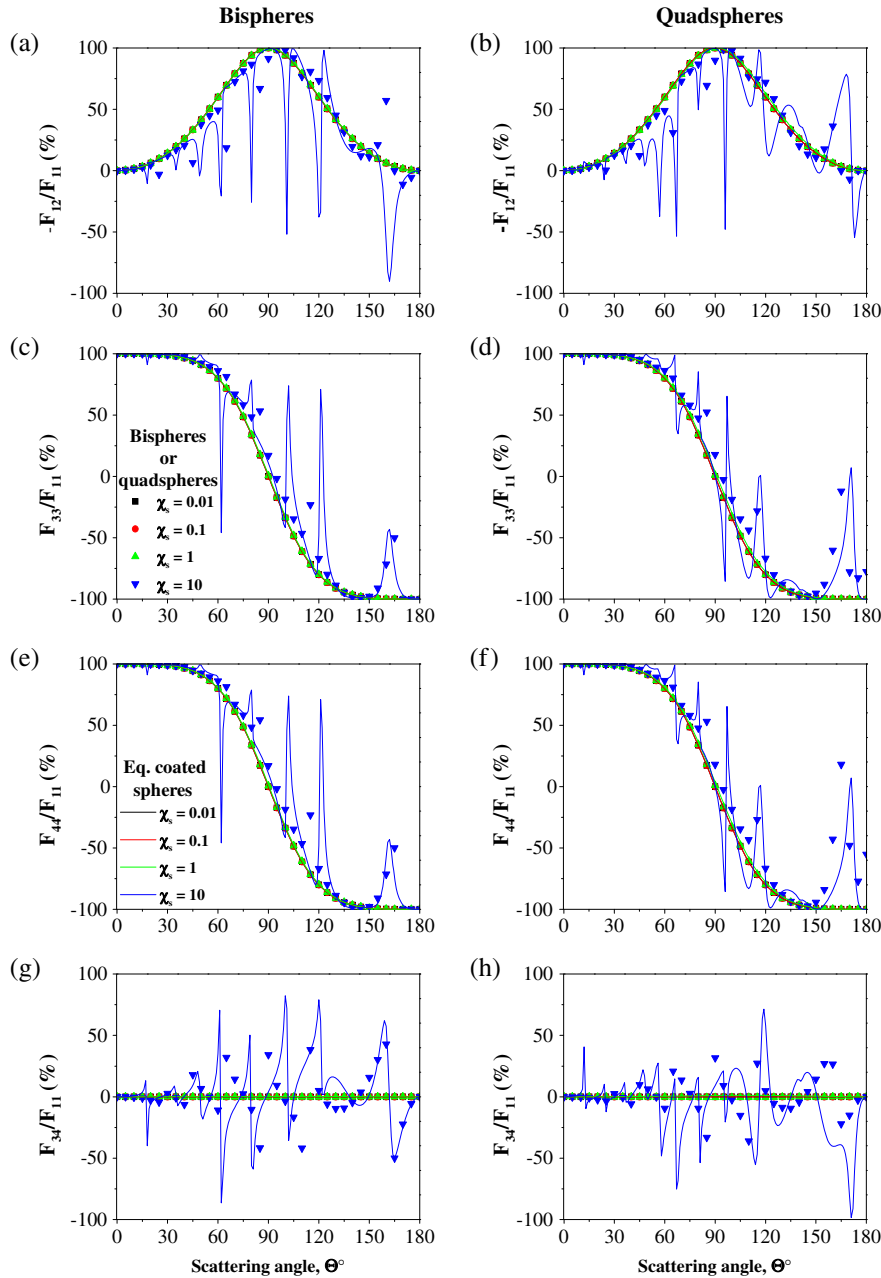


Fig. 9. Scattering matrix element ratios (a) and (b) $-F_{12}/F_{11}$, (c) and (d) F_{33}/F_{11} , (e) and (f) F_{44}/F_{11} , and (g) and (h) F_{34}/F_{11} as functions of scattering angle Θ obtained with the T-matrix method for bispheres and quadspheres and for the corresponding volume and average projected area equivalent coated spheres for monomer size parameters $\chi_s = 0.01, 0.1, 1$, and 10.

Fig. 5 were obtained for $k = 0.004$ while n increased from 1.03 to 1.2 and 1.5. For χ_s smaller than 0.1 and larger than 1, the relative error for any aggregate considered was less than 5% and 17% for n equal to 1.03 and 1.2, respectively. In the same χ_s range, the relative error for the bispheres, quadspheres, and rings of 10 and 20 spheres with $n = 1.5$ increased and reached up to 12%, 22%, 22%, and 44%, respectively.

Finally, the asymmetry factor did not change significantly when the monomers' relative refractive index n increased from 1.03 to 1.2 and their relative absorption index k varied from 0.004 to 0.1. However, for $n = 1.5$, the aggregates had smaller asymmetry factor than the volume and average projected area equivalent coated spheres for χ_s larger than 1.0.

Overall, approximating the integral radiation characteristics of bispheres by those of the volume and average projected area equivalent coated spheres was valid for all values of n , k , and χ_s considered. This approximation was also appropriate for quadspheres and rings of 10 and 20 spheres with relative refractive index n up to 1.2 and relative absorption index k up to 0.1 for monomer size χ_s between 0.01 and 10. This approximation became less accurate as the monomers' relative refractive index n and number N_s in the aggregates increased.

E. Aggregates of Polydisperse Monomers

The bispheres, quadspheres, and rings of 10 and 20 spheres considered so far consisted of monodisperse spherical monomers. However, the cells of cyanobacteria, such as

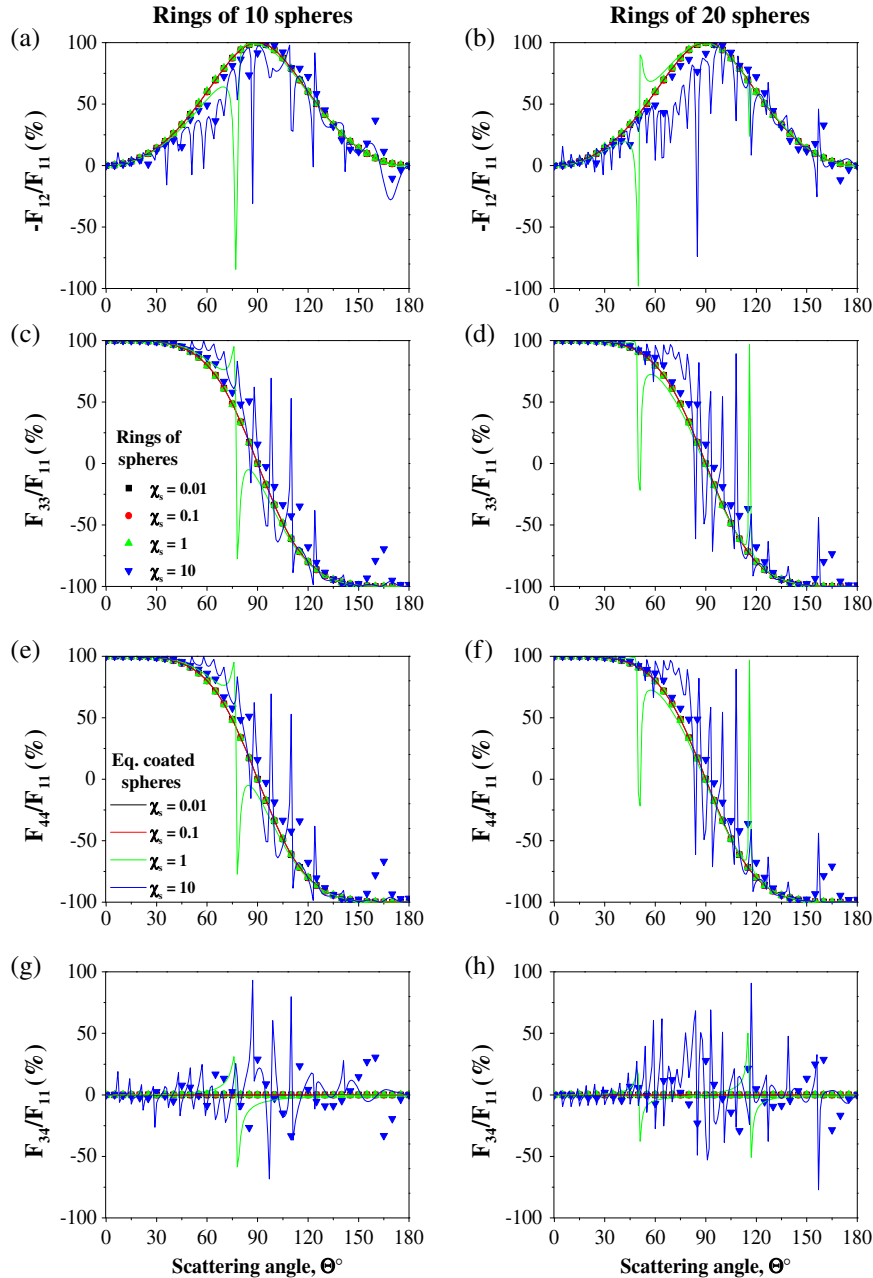


Fig. 10. Scattering matrix element ratios (a) and (b) $-F_{12}/F_{11}$, (c) and (d) F_{33}/F_{11} , (e) and (f) F_{44}/F_{11} , and (g) and (h) F_{34}/F_{11} as functions of scattering angle Θ obtained with the T-matrix method for rings of 10 spheres and 20 spheres, and for the corresponding volume and average projected area equivalent coated spheres for monomer size parameters $\chi_s = 0.01, 0.1, 1, \text{ and } 10$.

A. elenkini and *A. circularis*, are typically polydisperse, as illustrated in Fig. 1. Furthermore, the heterocyst present in some cyanobacteria are usually larger than the vegetative cells. This section assesses whether the volume and average projected area equivalent coated sphere approximation was also valid for rings of spheres consisting of polydisperse monomers.

Table 1 shows the schematics of the three different rings of spheres considered and their morphological features. The number of vegetative cells and heterocysts were respectively denoted by N_v and N_h such that $N_s = N_v + N_h$ while each cell type was monodisperse with size parameters χ_v and χ_h , respectively. Aggregate 1 consisted of 10 monomers including 2 heterocyst while Aggregates 2 and 3 had $N_s = 20$ monomers

with 2 and 1 heterocysts, respectively. The radius of the heterocysts in Aggregates 1 and 2 was taken to be 20% larger than that of the vegetative cells. The sizes and positions of the monomers in Aggregate 3 were derived using the micrograph reproduced in Fig. 1(d). In all cases, the size parameters χ_v and χ_h were larger than 5.0. The relative complex index of refraction was assumed to be $m = 1.03 + i0.004$ and identical for both vegetative cells and heterocysts. The average projected area of each of these aggregates was computed numerically to obtain the inner $r_{\bar{A}_p, \text{eq}, i}$ and outer $r_{\bar{A}_p, \text{eq}, o}$ radii of the corresponding volume V and average projected area \bar{A}_p of the equivalent coated sphere. Table 1 reports the absorption $\langle C_{\text{abs}}^a \rangle$ and scattering $\langle C_{\text{sca}}^a \rangle$ cross sections and the asymmetry factor g of the three randomly oriented aggregates predicted

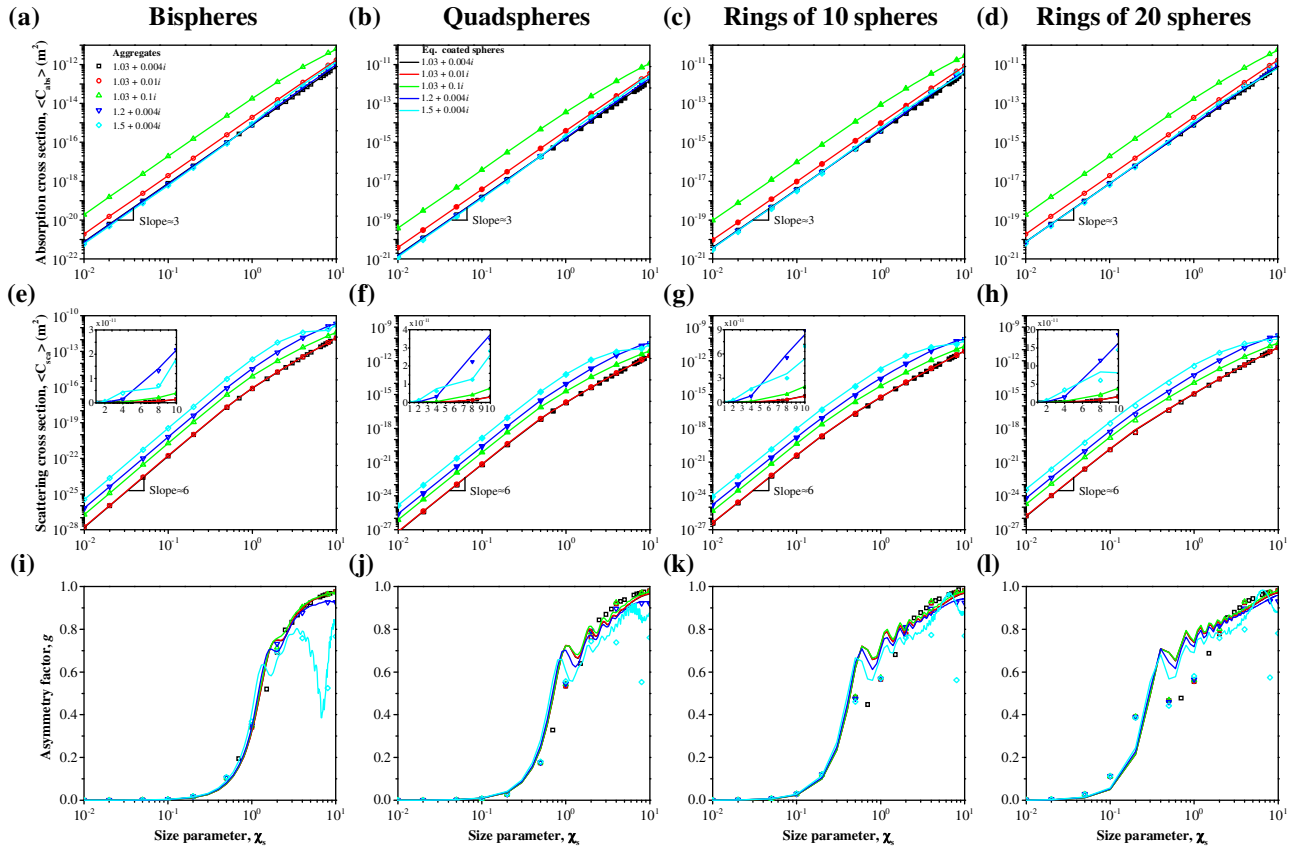
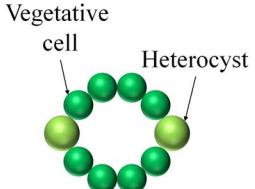


Fig. 11. (a)–(d) Absorption and (e)–(h) scattering cross sections and (i)–(l) asymmetry factors of bispheres, quadspheres, and rings of 10 and 20 spheres, respectively, as functions of monomer size parameters χ_s ranging from 0.01 to 10 and their corresponding volume and average projected area equivalent coated spheres with different complex indices of refraction.

Table 1. Comparison between Absorption and Scattering Cross Sections and Asymmetry Factor of Randomly Oriented Rings of Polydisperse Spherical Monomers and Their Volume and Average Projected Area Equivalent Coated Spheres^a

	Aggregate 1	Aggregate 2	Aggregate 3
Schematic			
χ_v/χ_h	8/9.6	8/9.6	5.3–10.6/9.4
N_v/N_h	8/2	18/2	19/1
V (μm^3)	30.6	57.3	57.1
\bar{A}_p (μm^2)	18.3	37.7	35.2
$\langle C_{\text{abs}}^a \rangle$ (μm^2)	2.24	4.19	4.16
$\langle C_{\text{sca}}^a \rangle$ (μm^2)	4.07	7.43	7.76
g	0.974	0.973	0.976
Volume and average projected area equivalent coated spheres			
$r_{\bar{A}_p, \text{eq}, i}$ (μm)	1.90	3.03	2.88
$r_{\bar{A}_p, \text{eq}, o}$ (μm)	2.42	3.46	3.35
$C_{\text{abs}/\text{sca}, V+\bar{A}_p}^{\text{CS}}$ (μm^2)	2.24	4.19	4.16
$C_{\text{abs}/\text{sca}, V+\bar{A}_p}^{\text{CS}}$ (μm^2)	4.11	7.38	7.72
g	0.971	0.971	0.972

^aHere also, $m = 1.03 + i0.004$.

by the superposition T-matrix method as well as those of the corresponding volume and average projected area equivalent coated spheres. They fell within 1% of each other for the three aggregates considered. In other words, the equivalent coated sphere approximation provided good estimates of $\langle C_{\text{abs}}^a \rangle$, $\langle C_{\text{sca}}^a \rangle$, and g for rings of polydisperse and optically soft spheres representative of multicellular cyanobacteria.

F. Computational Time

Computing the radiation characteristics of a bisphere, quad-sphere, and rings of $N_s = 10$ and 20 monodisperse spheres with $\chi_s = 10$ and $m = 1.03 + i0.004$ using the superposition T-matrix method required 9, 24, 227, and 2063 s, respectively, on a parallel computing cluster with 50 CPUs. By contrast, computing the radiation characteristics of the corresponding volume and average projected area equivalent coated spheres on a single dual core 2.53 GHz CPU required 1.3, 1.6, 2.9, and 3.3 μs , respectively. Note also that savings in computational time was found to increase as the size parameter χ_s and/or the number of monomers N_s increased. Thus, the proposed volume and average projected area equivalent coated spheres offers a way to estimate their absorption and scattering cross sections and their asymmetry factor rapidly and relatively accurately.

5. CONCLUSIONS

This study established that randomly oriented bispheres, quadspheres, and circular rings of spheres can be approximated as equivalent coated spheres with identical volume and average projected area for predicting the absorption and scattering cross sections and their asymmetry factor. This approximation was valid for monomer size parameter between 0.01 and 10 and for relative refractive index up to 1.2 and absorption index up to 0.1. The general trends in the scattering matrix element ratios of bispheres, quadspheres, and rings of spheres were similar to those of their volume and average projected area equivalent coated spheres except for oscillations observed for monomer size parameters larger than 1.0. This was attributed to internal reflection in the coating and its waveguiding effect. Overall, the equivalent coated sphere approximation offers a simple, rapid, and relatively accurate way of predicting the radiation characteristics of randomly oriented bispheres, quadspheres, and rings of spheres for a wide range of monomer number, size parameter, and relative complex index of refraction. It can be used for predicting the integral radiation characteristics of photosynthetic micro-organisms as well as for retrieving their optical properties and/or their average volume and projected area from radiation characteristic measurements.

ACKNOWLEDGMENTS

The computation for this study was performed on the Hoffman2 cluster hosted by the Academic Technology Services (ATS) at the University of California, Los Angeles.

REFERENCES

1. H. Canter-Lund and J. W. G. Lund, *Freshwater Algae: Their Microscopic World Explored* (Biopress Limited, 1995).
2. L. Rodolfi, G. Chini Zittelli, N. Bassi, G. Padovani, N. Biondi, G. Bonini, and M. R. Tredici, "Microalgae for oil: strain selection, induction of lipid synthesis and outdoor mass cultivation in a

- low-cost photobioreactor," *Biotechnol. Bioeng.* **102**, 100–112 (2009).
3. A. Richmond, *Handbook of Microalgal Culture: Biotechnology and Applied Phycology* (Blackwell Science, 2004).
4. D. Das and T. N. Veziroglu, "Hydrogen production by biological processes: a survey of literature," *Int. J. Hydrogen Energy* **26**, 13–28 (2001).
5. Y. Chisti, "Biodiesel from microalgae," *Biotechnol. Adv.* **25**, 294–306 (2007).
6. J. R. Benemann, "Production of nitrogen fertilizer with nitrogen-fixing blue-green algae," *Enzyme Microb. Technol.* **1**, 83–90 (1979).
7. E. W. Becker, *Microalgae: Biotechnology and Microbiology* (Cambridge University, 1994), Vol. **10**.
8. B. E. Schirmer, J. M. de Vos, A. Antonelli, and H. C. Bagheri, "Evolution of multicellularity coincided with increased diversification of cyanobacteria and the great oxidation event," *Proc. Natl. Acad. Sci.* **110**, 1791–1796 (2013).
9. T. Kaneko, S. Sato, H. Kotani, A. Tanaka, E. Asamizu, Y. Nakamura, N. Miyajima, M. Hirose, M. Sugiura, S. Sasamoto, T. Kimura, T. Hosouchi, A. Matsuno, A. Muraki, N. Nakazaki, K. Naruo, S. Okumura, S. Shimpo, C. Takeuchi, T. Wada, A. Watanabe, M. Yamada, M. Yasuda, and S. Tabata, "Sequence analysis of the genome of the unicellular cyanobacterium *Synechocystis* sp. strain PCC6803 II. Sequence determination of the entire genome and assignment of potential protein-coding regions," *DNA Res.* **3**, 109–136 (1996).
10. Y. Hihara, K. Sonoike, M. Kanehisa, and M. Ikeuchi, "DNA microarray analysis of redox-responsive genes in the genome of the cyanobacterium *Synechocystis* sp. strain PCC 6803," *J. Bacteriol.* **185**, 1719–1725 (2003).
11. D. Lagarde, L. Beuf, and W. Vermaas, "Increased production of zeaxanthin and other pigments by application of genetic engineering techniques to *Synechocystis* sp. strain PCC 6803," *Appl. Environ. Microbiol.* **66**, 64–72 (2000).
12. M. A. Vega-Palas, F. Madueño, A. Herrero, and E. Flores, "Identification and cloning of a regulatory gene for nitrogen assimilation in the cyanobacterium *Synechocystis* sp. strain PCC 7942," *J. Bacteriol.* **172**, 643–647 (1990).
13. M. G. Pinho, M. Kjos, and J. W. Veening, "How to get (a) round: mechanisms controlling growth and division of coccoid bacteria," *Nat. Rev. Microbiol.* **11**, 601–614 (2013).
14. I. Berman-Frank, P. Lundgren, and P. Falkowski, "Nitrogen fixation and photosynthetic oxygen evolution in cyanobacteria," *Res. Microbiol.* **154**, 157–164 (2003).
15. A. Tiwari and A. Pandey, "Cyanobacterial hydrogen production—a step towards clean environment," *Int. J. Hydrogen Energy* **37**, 139–150 (2012).
16. R. R. Bidigare, M. E. Ondrusek, J. H. Morrow, and D. A. Kiefer, "*In-vivo* absorption properties of algal pigments," *Proc. SPIE* **1302**, 290–301 (1990).
17. M. Jonasz and G. Fournier, *Light Scattering by Particles in Water: Theoretical and Experimental Foundations* (Academic, 2007).
18. L. Pilon, H. Berberoğlu, and R. Kandilian, "Radiation transfer in photobiological carbon dioxide fixation and fuel production by microalgae," *J. Quant. Spectrosc. Radiat. Transfer* **112**, 2639–2660 (2011).
19. J.-F. Cornet and C.-G. Dussap, "A simple and reliable formula for assessment of maximum volumetric productivities in photobioreactors," *Biotechnol. Prog.* **25**, 424–435 (2009).
20. H. Berberoğlu and L. Pilon, "Experimental measurement of the radiation characteristics of *Anabaena variabilis* ATCC 29413-U and *Rhodobacter sphaeroides* ATCC 49419," *Int. J. Hydrogen Energy* **32**, 4772–4785 (2007).
21. L. Pottier, J. Pruvost, J. Deremetz, J.-F. Cornet, J. Legrand, and C.-G. Dussap, "A fully predictive model for one-dimensional light attenuation by *Chlamydomonas reinhardtii* in a torus photobioreactor," *Biotechnol. Bioeng.* **91**, 569–582 (2005).
22. A. Quirantes and S. Bernard, "Light scattering by marine algae: two-layer spherical and nonspherical models," *J. Quant. Spectrosc. Radiat. Transfer* **89**, 311–321 (2004).
23. H. Berberoğlu, J. Yin, and L. Pilon, "Light transfer in bubble sparged photobioreactors for H₂ production and CO₂ mitigation," *Int. J. Hydrogen Energy* **32**, 2273–2285 (2007).

24. G. Mie, "Beiträge zur Optik trüber Medien, speziell kolloidaler Metallösungen," *Ann. Phys.* **330**, 377–445 (1908).
25. A. L. Aden and M. Kerker, "Scattering of electromagnetic waves from two concentric spheres," *J. Appl. Phys.* **22**, 1242–1246 (1951).
26. M. Kerker, *The Scattering of Light, and Other Electromagnetic Radiation* (Academic, 1969).
27. H. C. van de Hulst, *Light Scattering by Small Particles* (Courier Dover, 2012).
28. J. R. Wait, "Scattering of a plane wave from a circular dielectric cylinder at oblique incidence," *Can. J. Phys.* **33**, 189–195 (1955).
29. P. C. Waterman, "Matrix formulation of electromagnetic scattering," *Proc. IEEE* **53**, 805–812 (1965).
30. D. W. Mackowski, "Calculation of total cross sections of multiple-sphere clusters," *J. Opt. Soc. Am. A* **11**, 2851–2861 (1994).
31. M. I. Mishchenko, L. D. Travis, and A. A. Lacis, *Scattering, Absorption, and Emission of Light by Small Particles* (Cambridge University, 2002).
32. M. I. Mishchenko, D. W. Mackowski, and L. D. Travis, "Scattering of light by bispheres with touching and separated components," *Appl. Opt.* **34**, 4589–4599 (1995).
33. B. T. Draine, "The discrete-dipole approximation and its application to interstellar graphite grains," *Astrophys. J.* **333**, 848–872 (1988).
34. K. N. Liou, *An Introduction to Atmospheric Radiation* (Academic, 2002).
35. A. Bricaud and A. Morel, "Light attenuation and scattering by phytoplanktonic cells: a theoretical modeling," *Appl. Opt.* **25**, 571–580 (1986).
36. A. Quirantes and S. Bernard, "Light-scattering methods for modelling algal particles as a collection of coated and/or nonspherical scatterers," *J. Quant. Spectrosc. Radiat. Transfer* **100**, 315–324 (2006).
37. E. Lee, R.-L. Heng, and L. Pilon, "Spectral optical properties of selected photosynthetic microalgae producing biofuels," *J. Quant. Spectrosc. Radiat. Transfer* **114**, 122–135 (2013).
38. R. L. Heng, E. Lee, and L. Pilon, "Radiation characteristics and optical properties of filamentous cyanobacterium *Anabaena cylindrica*," *J. Opt. Soc. Am. A* **31**, 836–845 (2014).
39. E. Lee and L. Pilon, "Absorption and scattering by long and randomly oriented linear chains of spheres," *J. Opt. Soc. Am. A* **30**, 1892–1900 (2013).
40. C. F. Bohren and D. R. Huffman, *Absorption and Scattering of Light by Small Particles* (Wiley, 1998).
41. M. Modest, *Radiative Heat Transfer*, 2nd ed. (Academic, 2003).
42. S. Manickavasagam and M. P. Mengüç, "Scattering-matrix elements of coated infinite-length cylinders," *Appl. Opt.* **37**, 2473–2482 (1998).
43. H. R. Gordon, "Light scattering and absorption by randomly-oriented cylinders: dependence on aspect ratio for refractive indices applicable for marine particles," *Opt. Express* **19**, 4673–4691 (2011).
44. M. I. Mishchenko, G. Videen, V. A. Babenko, N. G. Khlebtsov, and T. Wriedt, "T-matrix theory of electromagnetic scattering by particles and its applications: a comprehensive reference database," *J. Quant. Spectrosc. Radiat. Transfer* **88**, 357–406 (2004).
45. B. N. Khlebtsov, V. A. Khanadeyev, J. Ye, D. W. Mackowski, G. Borghs, and N. G. Khlebtsov, "Coupled plasmon resonances in monolayers of metal nanoparticles and nanoshells," *Phys. Rev. B* **77**, 035440 (2008).
46. L. L. Zhao, K. L. Kelly, and G. C. Schatz, "The extinction spectra of silver nanoparticle arrays: influence of array structure on plasmon resonance wavelength and width," *J. Phys. Chem. B* **107**, 7343–7350 (2003).
47. H. Kimura, L. Kolokolova, and I. Mann, "Optical properties of cometary dust: constraints from numerical studies on light scattering by aggregate particles," *Astron. Astrophys.* **407**, L5–L8 (2003).
48. D. W. Mackowski and M. I. Mishchenko, "Calculation of the T matrix and the scattering matrix for ensembles of spheres," *J. Opt. Soc. Am. A* **13**, 2266–2278 (1996).
49. M. P. Mengüç, S. Manickavasagam, and D. A. D'Sa, "Determination of radiative properties of pulverized coal particles from experiments," *Fuel* **73**, 613–625 (1994).
50. K. N. Liou and Y. Takano, "Light scattering by nonspherical particles: remote sensing and climatic implications," *Atmos. Res.* **31**, 271–298 (1994).
51. F. M. Kahnert, J. J. Stannnes, and K. Stannnes, "Can simple particle shapes be used to model scalar optical properties of an ensemble of wavelength-sized particles with complex shapes?" *J. Opt. Soc. Am. A* **19**, 521–531 (2002).
52. P. Yang, G. W. Kattawar, and W. J. Wiscombe, "Effect of particle asphericity on single-scattering parameters: comparison between platonic solids and spheres," *Appl. Opt.* **43**, 4427–4435 (2004).
53. P. Latimer, "Experimental tests of a theoretical method for predicting light scattering by aggregates," *Appl. Opt.* **24**, 3231–3239 (1985).
54. B. L. Drolen and C. L. Tien, "Absorption and scattering of agglomerated soot particulate," *J. Quant. Spectrosc. Radiat. Transfer* **37**, 433–448 (1987).
55. K. Kumar, C. N. Dasgupta, B. Nayak, P. Lindblad, and D. Das, "Development of suitable photobioreactors for CO₂ sequestration addressing global warming using green algae and cyanobacteria," *Biores. Technol.* **102**, 4945–4953 (2011).
56. D. J. Brown and G. T. Vickers, "The use of projected area distribution functions in particle shape measurement," *Powder Technol.* **98**, 250–257 (1998).
57. D. W. Mackowski and M. I. Mishchenko, "A multiple sphere T-matrix Fortran code for use on parallel computer clusters," *J. Quant. Spectrosc. Radiat. Transfer* **112**, 2182–2192 (2011).
58. C. Mätzler, "MATLAB functions for Mie scattering and absorption, version 2," Institut für Angewandte Physik Research Report No. 2002–11, Vol. **8** (University of Bern, 2002).
59. T. L. Farias, Ü. Ö. Köylü, and M. G. Carvalho, "Range of validity of the Rayleigh-Debye-Gans theory for optics of fractal aggregates," *Appl. Opt.* **35**, 6560–6567 (1996).
60. R. A. West, "Optical properties of aggregate particles whose outer diameter is comparable to the wavelength," *Appl. Opt.* **30**, 5316–5324 (1991).
61. L. Liu and M. I. Mishchenko, "Effects of aggregation on scattering and radiative properties of soot aerosols," *J. Geophys. Res.* **110**(D11), 16 (2005).